Search for heavy neutral leptons in decays of W bosons using a dilepton displaced vertex in $\sqrt{s} = 13$ TeV pp collisions with the ATLAS detector

The ATLAS Collaboration

A search for a long-lived, heavy neutral lepton ($\mathcal{N}$) in 139 fb^{-1} of $\sqrt{s} = 13$ TeV pp collision data collected by the ATLAS detector at the Large Hadron Collider is reported. The $\mathcal{N}$ is produced via $W \to \mathcal{N}\mu$ or $W \to \mathcal{N}e$ and decays into two charged leptons and a neutrino, forming a displaced vertex. The $\mathcal{N}$ mass is used to discriminate between signal and background. No signal is observed, and limits are set on the squared mixing parameters of the $\mathcal{N}$ with the left-handed neutrino states for the $\mathcal{N}$ mass range 3 GeV $< m_{\mathcal{N}} < 15$ GeV. For the first time, limits are given for both single-flavor and multiflavor mixing scenarios motivated by neutrino flavor oscillation results for both the normal and inverted neutrino-mass hierarchies.

The observations of neutrino flavor oscillations [1, 2] can be explained by postulating the existence of right-handed neutrino states that carry no Standard Model (SM) gauge charges, allowing them to have Majorana masses. The resulting "type-I seesaw" model [3–9] explains the light neutrino masses and predicts heavy mass eigenstates, referred to as "heavy neutral leptons" (HNLs) and denoted by $\mathcal{N}$ henceforth. The existence of HNLs can also explain the baryon asymmetry of the universe via leptogenesis [10–12], which is efficient for HNL masses down to the sub-GeV range [13–17]. Moreover, a model with three HNLs can incorporate a dark matter candidate [14, 18–21].

Each HNL state carries a small admixture of the left-handed neutrino of flavor $\alpha = \{e, \mu, \tau\}$. It can therefore participate in weak interactions, controlled by dimensionless mixing coefficients U_α, where $|U_\alpha| \ll 1$. Previous searches were interpreted only in terms of a one-HNL model with single-flavor mixing (1SFH) [22–30]. This model is a useful benchmark but is not phenomenologically viable as it predicts neutrino masses that are too large and does not account for two neutrino mass splittings or neutrino flavor oscillations [31–33]. The simplest viable model is that of two quasi-degenerate HNLs (2QDH), with close masses and couplings, where all U_α are nonzero. A reinterpretation of ATLAS HNL searches in such HNL scenarios has been performed [33]. However, no experiment has directly explored 2QDH models yet.

The search reported here considers the production of HNLs via $W \to \mathcal{N}\ell_\alpha$, where $\alpha = \{e, \mu\}$ indicates the flavor of the "prompt" lepton ℓ_α. The HNL decays into two oppositely charged leptons and a neutrino: $\mathcal{N} \to \ell_\beta \ell_\gamma \nu_\gamma$ via an intermediate W^* boson, or $\mathcal{N} \to \nu_\beta \ell_\gamma \ell_\gamma$ via a Z^* boson, where $\beta, \gamma = e$ or μ. The search focuses on the mixing and mass range (up to 20 GeV) in which the HNL is long-lived. The resulting HNL lifetime can be approximated by $\tau_\mathcal{N} \approx (4.3 \times 10^{-12}\ \text{s})|U|^{-2}(m_\mathcal{N}/1\ \text{GeV})^{-5}$ [34] where $|U|^2 \equiv \sum_\beta |U_\beta|^2$, is taken from Ref. [35]. The HNL decay occurs at a significantly displaced position from the proton–proton (pp) collision point, forming a displaced vertex (DV) of two charged leptons, $\ell_\beta \ell_\gamma$ or $\ell_\gamma \ell_\gamma$. The measured final states are labeled according to the prompt and displaced charged leptons therein, denoted by "ℓ_α–$\ell_\beta \ell_\gamma$" (explicitly listed in Table 1). Decays of the W or $\mathcal{N}$ to τ-leptons were determined to have negligible impact on the analysis, since the leptonic branching fractions of the τ and the soft lepton spectrum make their selection highly inefficient. In 1SFH scenarios, the analysis is sensitive to the squared mixing parameter $|U_\mu|^2$ via the final states μ–$\mu\mu$, μ–μe, and μ–ee, while $|U_e|^2$ is accessible via e–ee, e–$e\mu$, and e–$\mu\mu$. In 2QDH scenarios, the combination of the six final states provides sensitivity to $|U_e|^2$, $|U_\mu|^2$, and $|U_\tau|^2$. For both scenarios, bounds on the mixing parameters are extracted in the "Dirac limit" of lepton-number-conserving (LNC) HNL interactions, where the W^*-mediated final state is $\ell_\alpha^\pm$–$\ell_\alpha^\mp \ell_\gamma^\pm$, and in the "Majorana limit" of equal branching fractions for LNC and lepton-number-violating (LNV, $\ell_\alpha^\pm$–$\ell_\beta^\pm \ell_\gamma^\mp$) decays [36]. The analysis can separate LNC and LNV decays only by using an explicit charge requirement for the 1SFH model in the μ–μe and e–$e\mu$ channels, where the displaced leptons are experimentally distinguishable. The bounds are tighter than and supersede those of Ref. [22], where only the final states μ–$\mu\mu$ and μ–μe were studied.

This search is performed with 139 fb^{-1} of 13 TeV pp collision data collected by the ATLAS experiment at the LHC from 2015 to 2018. To study the signal sensitivity, Monte Carlo (MC) signal samples were generated using Pythia 8.212 [37] with the A14 set of tuned parameters [38] and the NNPDF2.3lo PDF set [39]. The impact of multiple pp interactions per bunch crossing was modeled by adding simulated minimum-bias events generated with Pythia 8.210 using the A3 tune [40] and NNPDF2.3lo PDF set. Particles were propagated through a detector simulation [41] based on Geant4 [42]. To properly simulate spin correlations between W-boson decay products [33, 43, 44], which are not accounted for in Pythia 8, events are weighted to reproduce the angular distributions obtained with MadGraph5_aMC@NLO 2.9.3 [45] using the HeavyN model [46, 47]. The weighting procedure is validated by comparing the momentum spectra of each of the charged-lepton flavors and the neutrino between the weighted Pythia 8 and

MadGraph5_aMC@NLO samples. For each ℓ_α–$\ell_\beta\ell_\gamma$ final state, signal samples were generated with HNL masses in the range 3 GeV $< m_N <$ 20 GeV and proper decay lengths $c\tau_N = 1, 10, 100$ mm.

The ATLAS detector [48–50] is a cylindrical detector with forward-backward symmetry and nearly 4π solid-angle coverage.[1] It is composed of three major subsystems: the inner detector (ID) closest to the pp interaction point (IP), the electromagnetic and hadronic calorimeters, and the muon spectrometer farthest from the IP. The ID is used to reconstruct the trajectories of charged particles (tracks) in an almost uniform 2 T magnetic field, and comprises three subsystems: pixel, silicon microstrip tracker (SCT) and transition radiation tracker. An extensive software suite [51] is used in the reconstruction and analysis of data and MC events, in detector operations, and in the trigger and data acquisition systems of the experiment.

Events in the signal region (SR) of this analysis were selected with triggers [52] that require a single isolated electron [53] or muon [54] with a minimum transverse momentum (p_T) of 20–26 GeV, depending on the lepton flavor and year. Events passing the trigger are required by a filter algorithm to contain at least one lepton [55, 56] with $p_T > 28$ GeV and $|\eta| < 2.5$.

To ensure isolation of this lepton from hadronic activity, the scalar sum of the p_T of other tracks within a cone of size $\Delta R = 0.3$ around the lepton momentum ($\Sigma p_T^{(0.3)}$) is required to be less than 5% of the lepton p_T. The filter also requires at least one additional lepton with $p_T > 5$ GeV, $|\eta| < 2.5$, and $\Sigma p_T^{(0.3)}/p_T < 1.0$. To reduce the number of events with prompt decays while maintaining efficiency for displaced leptons, the second lepton must have a transverse impact parameter (d_0) with respect to the IP of $|d_0| > 0.1$ mm ($|d_0| > 1$ mm) for muons (electrons). Events that pass the filter are then processed with a large-radius tracking (LRT) algorithm [57], that is efficient for tracks with $|d_0| < 300$ mm. The LRT is run after standard tracking [58], which is efficient only for $|d_0| < 10$ mm. Standard and large-radius tracks are combined with muon-spectrometer tracks (electromagnetic energy clusters) to reconstruct muons (electrons). Events are required to contain a reconstructed primary vertex (PV) with at least two tracks, each having $p_T > 500$ MeV. When more than one PV is reconstructed, the one with the highest Σp_T^2 is used, where the sum is over the tracks associated with the PV.

Event selection relies on the reconstruction of two physics objects: a prompt lepton and a DV. The prompt-lepton candidate, ℓ_α, is taken to be the highest-p_T muon (electron) that satisfies $p_T > 3$ (4.5) GeV, $|d_0| < 3$ mm, and $|(z_0 - z_{PV})\sin\theta| < 0.5$ mm, where z_0 is the track's longitudinal impact parameter and z_{PV} is the z coordinate of the PV. If a prompt muon and a prompt electron have an angular separation $\Delta R < 0.05$, the event is rejected. Reconstruction of DVs is performed with an optimized version of the secondary vertexing algorithm described in Ref. [59]. First, "seed" DVs are formed from pairs of tracks from both the standard tracking and LRT algorithms. Subsequently, tracks are added to the DVs, and closely spaced DVs are merged. The secondary vertexing is run with the following configuration changes relative to Ref. [59]: seed DVs are formed from leptons only, with at least one lepton satisfying $|d_0| > 1$ mm, and each having at least eight pixel plus SCT hits; leptonic and hadronic tracks are subsequently attached to the DVs, but selected DVs must have exactly two leptons and no additional tracks.

Events must contain a prompt lepton and a DV comprising a pair of leptons with opposite-sign (OS) electric charge, although same-sign (SS) DVs are retained and used for background studies. If a displaced track is identified as both a muon and an electron, the track is taken to be either a muon or an electron based on its muon- and electron-identification quality, and for DVs with electrons, quality criteria optimized

---

[1] ATLAS uses a right-handed coordinate system with its origin at the nominal IP in the center of the detector and the z-axis along the beam pipe. The x-axis points from the IP to the center of the LHC ring, and the y-axis points upward. Cylindrical coordinates (r, ϕ) are used in the transverse plane, ϕ being the azimuthal angle around the z-axis. The pseudorapidity is defined in terms of the polar angle θ as $\eta = -\ln\tan\theta/2$. Angular distance is measured in units of $\Delta R \equiv \sqrt{(\Delta\eta)^2 + (\Delta\phi)^2}$.

for displaced tracks are applied [60]. If a displaced track in the DV is within $\Delta R = 0.05$ of the prompt lepton, the event is rejected. The DV radial position (r_{DV}) must satisfy 4 mm < r_{DV} < 300 mm. The invariant mass of the DV and the prompt lepton, which is generally smaller than the W mass, must satisfy 40 GeV < $m_{DV+\ell}$ < 90 GeV.

Background arises from five sources: DVs from particle interactions with detector material; decays of metastable SM particles; $Z \to \ell\ell$ decays; cosmic-ray muons; and DVs from random crossings of lepton tracks. The following SR selection is designed to retain high signal efficiency and suppress the first four types of background to negligible levels, with random-crossing remaining the dominant background. Cosmic-ray muons, which can be reconstructed as two back-to-back muons in a DV, are rejected by requiring the two displaced tracks to satisfy $\sqrt{(\Sigma\eta)^2 + (\pi - \Delta\phi)^2} > 0.05$ [61]. Dielectron (ee) DVs have the most background from particle interactions with detector material, so those selected must be in regions without detector material, determined from a three-dimensional map of the ID [62]. The displaced dilepton's invariant mass (m_{DV}), which is generally smaller than m_N due to the unobserved final-state neutrino, is used to suppress background from J/ψ and other heavy-flavor decays. For $\mu\mu$ DVs, m_{DV} > 5.5 GeV is required. For $e\mu$ and ee DVs, the selection efficiency is smaller, motivating looser requirements that exploit correlations between r_{DV} and m_{DV}. These requirements are: m_{DV} > 5.5 GeV for r_{DV} < (225/7) mm; m_{DV} > 2 GeV for r_{DV} > (750/7) mm; and m_{DV} > 7 GeV × (1 − r_{DV}/(150 mm)) between these r_{DV} regions [36].

Background from $Z \to \ell\ell$ decays, in which one of the leptons forms a DV with a third lepton, is suppressed by vetoing events where the invariant mass of the prompt lepton and the displaced lepton with the same flavor (i.e., $\alpha = \beta$) and opposite charge satisfies 80 GeV < $m(\ell_\alpha^\pm \ell_\beta^\mp)$ < 100 GeV. In channels with $e\mu$ DVs, the random crossing background is reduced by roughly 50% for 1SFH, LNC interpretations, by requiring the prompt and displaced lepton with the same-flavor to have opposite charges : $\mu^\pm - \mu^\mp e^\pm$ or $e^\pm - e^\mp \mu^\pm$.

The four-momentum of the HNL is obtained by applying four-momentum conservation in the W and N decays, using the kinematics of the charged leptons, the known W mass, an approximation where the leptons and neutrino are massless, and the flight direction of the N, given by the vector connecting the PV and DV [36]. This calculation yields a quadratic equation with two solutions. The positive-radical solution is used to define the invariant mass (m_{HNL}) of the HNL candidate. In MC signal events, the distribution of m_{HNL} peaks at the generated value m_N, as shown in Figure 1(a).

The final SR selection is m_{HNL} < 20 GeV. The maximum signal selection efficiency is approximately 4%. A control region (CR) is defined as events with 20 GeV < m_{HNL} < 50 GeV. Since HNLs with m_N > 20 GeV and $|U_\alpha|^2$ values that the search is sensitive to are short-lived, they fail the r_{DV} requirements, resulting in negligible signal contamination in the CR.

A validation region (VR) is used for data-driven background modeling and evaluation of systematic uncertainties. The VR comprises events that passed a variety of triggers, underwent LRT reconstruction, and do not contain a prompt lepton. The DVs in the VR must satisfy the r_{DV} requirements and pass the cosmic-ray muon veto. For ee DVs, the detector material veto is also applied. The expected signal contamination in the VR is less than two events for a 100% HNL branching fraction into the channel of interest. Since the VR contains more than 100 events in each DV channel, the signal contamination is negligible.

Background from random track crossings is expected to yield equal numbers of OS and SS DVs, given the large number of tracks produced in each event. By contrast, background from $Z \to \ell\ell$ or cosmic-ray muons yields only OS DVs, and backgrounds from particle interactions with detector material or from decays of metastable hadrons preferentially yield OS DVs. Figure 1(b) shows the m_{DV} distributions for SS

and OS DVs in the VR. Good agreement is seen between the yield and shape of the distributions, shown for $e\mu$ DVs. This indicates that the dominant source of background in the SR is random lepton crossings. Therefore, the background model described next focuses on this background type. A systematic uncertainty related to this assumption is described below.
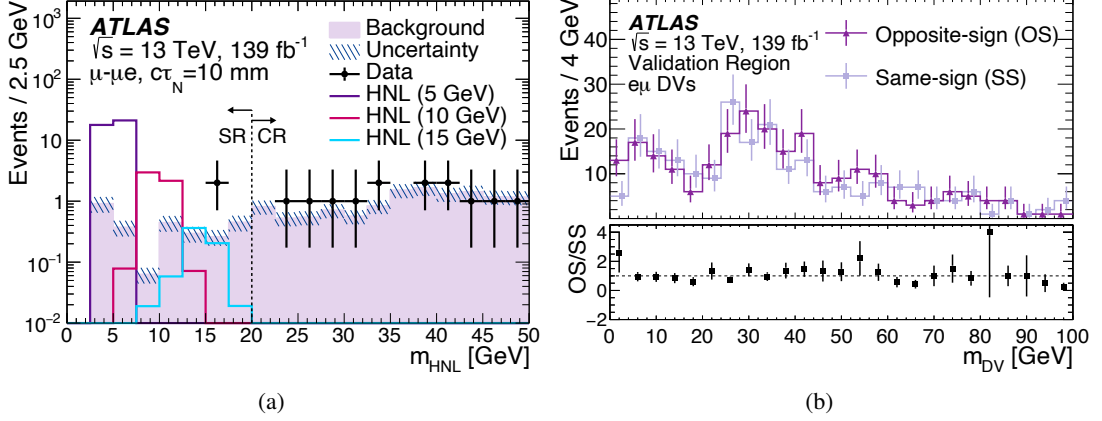

Figure 1: (a) The m_{HNL} distribution in the signal (SR) and control (CR) regions for the observed data, the shuffled-event-model background normalized by the fit described in the text with its uncertainty, and simulated signal for three different mass hypotheses. (b) The m_{DV} distributions for the OS and SS $e\mu$ DVs in the validation region. The marker is offset from the central position for visualization purposes.

The signal and background yields are obtained with the following fit. The fit uses a data-driven background model obtained from a sample of "shuffled events". This sample is created by combining each OS DV in the VR with each prompt lepton found in a non-VR event that contains an SS DV satisfying loose requirements: $m_{\text{DV}} > 1$ GeV, with no lepton identification criteria imposed on its displaced leptons. For each channel, the shuffled sample has at least 2×10^3 times the number of events in the "unshuffled" data sample, in which the DV and the prompt lepton are from the same event. As with an unshuffled event, a shuffled event may have $m_{\text{HNL}} < 20$ GeV (SR) or 20 GeV $< m_{\text{HNL}} < 50$ GeV (CR). The background model in the SR and CR is given by the shuffled events (shown in Figure 1(a)) with an independent floating normalization factor for each channel. The signal model for the fit is taken from simulation and is assigned a single floating signal strength for all channels. The input to the fit is the OS-event yields observed in the SR and CR. Inclusion of the CR in the fit directly constrains the predicted background yield in the SR.

The shuffled-event background model relies on the assumption that the absence of correlation between the randomly crossing tracks results in an absence of correlation between the DV and the prompt lepton. The validity of this assumption is checked by comparing the m_{HNL} distributions and the $m_{\text{DV}+\ell}$ distributions of shuffled events with the distributions of unshuffled events. Only SS DVs are used in this test. In order to have a sufficient number of unshuffled events, the requirements on m_{HNL}, $m(\ell_\alpha^\pm \ell_\beta^\mp)$, and $m_{\text{DV}+\ell}$ are removed, and that on m_{DV} is loosened to $m_{\text{DV}} > 2$ GeV. The unshuffled-event samples have between 36 and 187 events in each channel, and the shuffled-event samples are more than 50 times larger. The comparison based on a Kolmogorov–Smirnov test yields probabilities ranging from 20% to 99% for the different channels, indicating the validity of the no-correlation assumption.

Systematic uncertainties in the background model, taken to be 100% correlated between the CR and the SR, are evaluated for two sources. The first estimates the uncertainty from the assumption that nonrandom

backgrounds are negligible, and is estimated from differences between the m_{HNL} distributions of shuffled events created from SS and OS DVs. This uncertainty varies between 5% for the $e{-}e\mu$ channel and 79% for the $\mu{-}\mu\mu$ channel. The second uncertainty accounts for statistical fluctuations in the m_{HNL} distribution of the shuffled sample due to the finite number of prompt leptons used therein. It is estimated from the differences between the m_{HNL} distributions for shuffled events of two types: in type 1 (2), the combined DV and prompt lepton originate from events in identical (different) DV channels (ee, $\mu\mu$, $e\mu$). This uncertainty is largest for the $\mu{-}\mu e$ channel, reaching 5%.

The total systematic uncertainty of the signal efficiency varies between 8% and 42% depending on the channel, $m_{\mathcal{N}}$, and $c\tau_{\mathcal{N}}$. Its largest contribution (up to 28%) arises from the reconstruction of displaced tracks and vertices. This is evaluated by comparing $K_{\mathrm{S}}^0 \to \pi^+\pi^-$ event yields in the VR with those in MC samples produced with PYTHIA 8.186 in bins of p_{T} and r_{DV}, as in Ref. [63]. An additional uncertainty of 3% in the track reconstruction efficiency is calculated by randomly removing tracks from each signal MC event with a p_{T}- and η-dependent probability [64].

Uncertainties due to data–MC differences in the trigger efficiency [53, 54] range up to 1%, and those due to lepton reconstruction, identification, and impact parameter resolution are between 2% and 17% [56, 65] for the different channels. As in Ref. [60], an uncertainty in lepton-identification is estimated as the difference in selection efficiency between large and small $|d_0|$ tracks. Its maximal value is 7%. The uncertainty in the W-boson production cross section and modeling is 3% [66], and that in the HNL branching fractions and decay modeling is 5%, arising mainly from the QCD corrections to the HNL hadronic decay width [35, 67]. Other uncertainties, including the impact of pileup on signal selection, luminosity uncertainty [68, 69], and uncertainty from the filtering selection used for the extended track reconstruction, each contribute at < 3%.

Table 1 shows the post-fit estimated and observed yields in the SR and CR for all channels (including the 1SFH, LNC scenario with the requirement $\ell_\alpha^\pm{-}\ell_\alpha^\mp\ell_\gamma^\pm$); a signal plus background hypothesis is used (post-fit signal is compatible with zero). The SR contains two OS events in each of the $e{-}ee$, $\mu{-}\mu e$, and $\mu{-}\mu\mu$ channels and one OS event in each of the $\mu{-}ee$ and $e{-}\mu\mu$ channels. No OS $e{-}e\mu$ events are observed. These yields are consistent with the estimated backgrounds shown. The observed yields in the CR are consistent with the CR background estimates.

Table 1: Numbers (yields) of estimated post-fit background events and of observed events in the signal and control regions. The background yields shown are from the 2QDH, inverted-hierarchy, Majorana-limit fit described in the text, and include both systematic and statistical uncertainties. The observed yields are shown for all final states. The last two rows show the 1SFH Dirac-limit, LNC configuration $\ell_\alpha^\pm{-}\ell_\alpha^\mp\ell_\gamma^\pm$.

Channel	Signal region		Control region	
	Background	Observed	Background	Observed
$e{-}ee$	0.4 ± 0.3	2	3.6 ± 1.8	2
$\mu{-}ee$	0.2 ± 0.1	1	1.8 ± 1.3	1
$e{-}e\mu$	0.9 ± 0.4	0	4.1 ± 1.9	5
$\mu{-}\mu e$	2.8 ± 0.8	2	12.2 ± 3.2	13
$e{-}\mu\mu$	1.2 ± 0.9	1	2.8 ± 1.6	3
$\mu{-}\mu\mu$	2.2 ± 1.4	2	8.7 ± 2.9	9
$e^\pm{-}e^\mp\mu^\pm$	0.6 ± 0.3	0	2.4 ± 1.4	3
$\mu^\pm{-}\mu^\mp e^\pm$	1.9 ± 0.6	0	8.1 ± 2.6	10

Limits are set at 95% confidence level (CL) on $|U_\alpha|^2$ vs. $m_\mathcal{N}$ for each HNL scenario, using the CL_s prescription [70] implemented in TRExFitter [71–73]. All systematic uncertainties are included in the fit by using nuisance parameters, whose post-fit values do not show any significant pull or constraint. Each MC signal sample corresponds to specific values of $|U_\alpha|^2$ vs. $m_\mathcal{N}$, for which the efficiency is evaluated and a hypothesis test is performed with 10^4 pseudoexperiments.

Figure 2 shows the excluded parameter space in the 1SFH and 2QDH scenarios for both the Dirac limit and the Majorana limit. In the 2QDH scenarios, exclusion limits are shown for the two neutrino-mass hierarchy scenarios. In the inverted-hierarchy case, the relative mixing coefficients are taken to be $x_\alpha \equiv |U_\alpha|^2/|U|^2 = 1/3$ ($\alpha = e, \mu, \tau$); for the normal-hierarchy case, the values $x_e = 0.06$, $x_\mu = 0.48$ and $x_\tau = 0.46$ are used [33, 74]. These values are at the centers of the regions consistent with the neutrino flavor oscillation data. The observed limits are consistent with the expected limits. The feature visible near $m_\mathcal{N} = 5$ GeV is due to the r_{DV}-dependent m_{DV} selection, which limits the sensitivity at low mass.
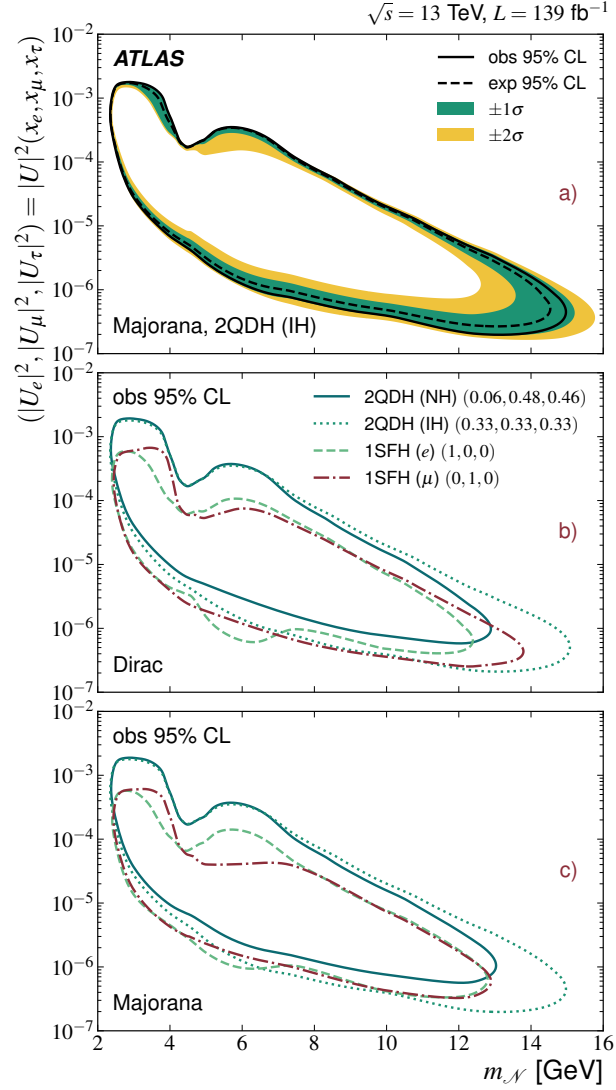
Figure 2: (a) The observed and expected 95% CL limits on $|U_\alpha|^2$ vs. $m_\mathcal{N}$ in the Majorana-limit case, with green and yellow bands showing the one and two standard deviation (σ) spreads for the expected limits. (b,c) The observed limits in the 2QDH scenario with inverted (IH) and normal (NH) mass hierarchy, and in 1SFH scenarios where the HNL mixes with only ν_μ or ν_e.

In conclusion, a search for long-lived heavy neutral leptons is conducted in a 139 fb^{-1} data sample of $\sqrt{s}$ = 13 TeV pp collisions collected with the ATLAS detector at the LHC. No excess is observed, and limits are set at 95% CL on the squared mixing coefficient $|U_\alpha|^2$ in different HNL scenarios for HNL masses in the approximate range 3 GeV $< m_\mathcal{N} <$ 15 GeV. The observed limits exclude a region with wider ranges of $|U_\mu|^2$ and $m_\mathcal{N}$ than previously excluded by ATLAS, and the limits on $|U_e|^2$ are novel in ATLAS. For the first time, limits are evaluated for the case of multiflavor mixing scenarios that agree with the neutrino flavor oscillation data, for both the normal and inverted neutrino-mass hierarchies. The strongest limits are observed for multiflavor mixing with the inverted hierarchy.
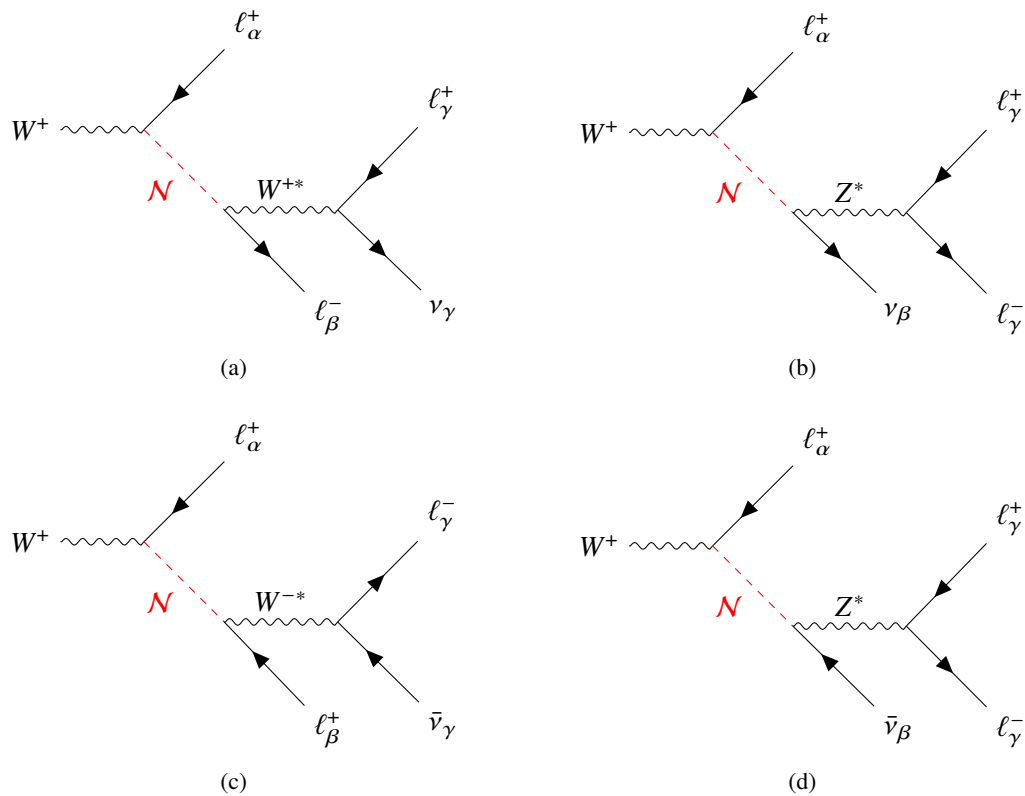
Appendix

Figure 3: Feynman diagrams for the HNL production and decay modes targeted in this analysis. The flavors of the leptons in the diagrams, labeled by α, β, and γ, are either muons or electrons. If the charged leptons in the HNL decay have the same flavor, then both the diagrams with the virtual W (a,c) and virtual Z (b,d) contribute to the process. Lepton number conserving (a,b) and lepton number violating (c,d) processes are shown. Equivalent processes are also valid for an initial state W^- boson.
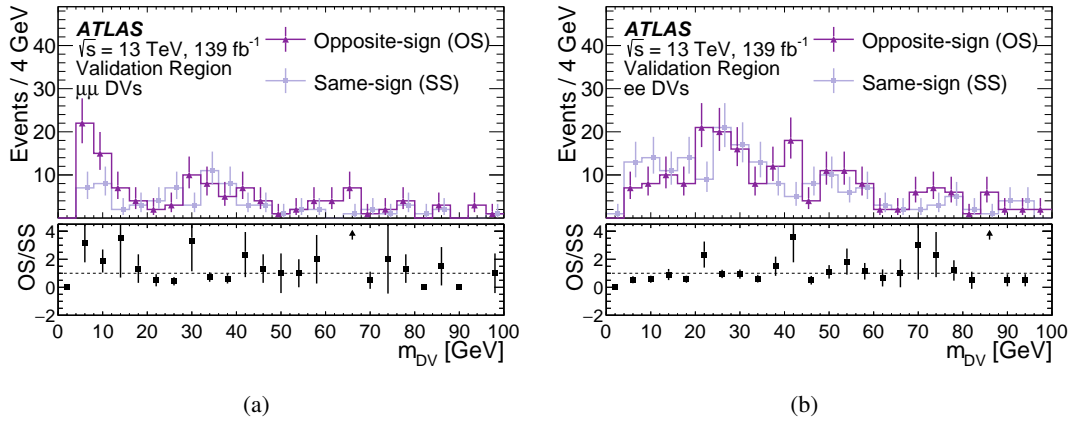
Figure 4: The m_{DV} distributions of OS and SS DVs in the validation region, for (a) $\mu\mu$ and (b) ee DVs. These demonstrate that the SS and OS DV distributions generally agree well, in line with the assumption that the dominant residual background for the search is that of random-crossing vertices, which is then estimated by a data-driven method. The disagreements which are visible here in part result from the remaining nonrandom-crossing backgrounds and these are accounted for with a systematic uncertainty. The markers are offset from the central positions for visualization purposes.
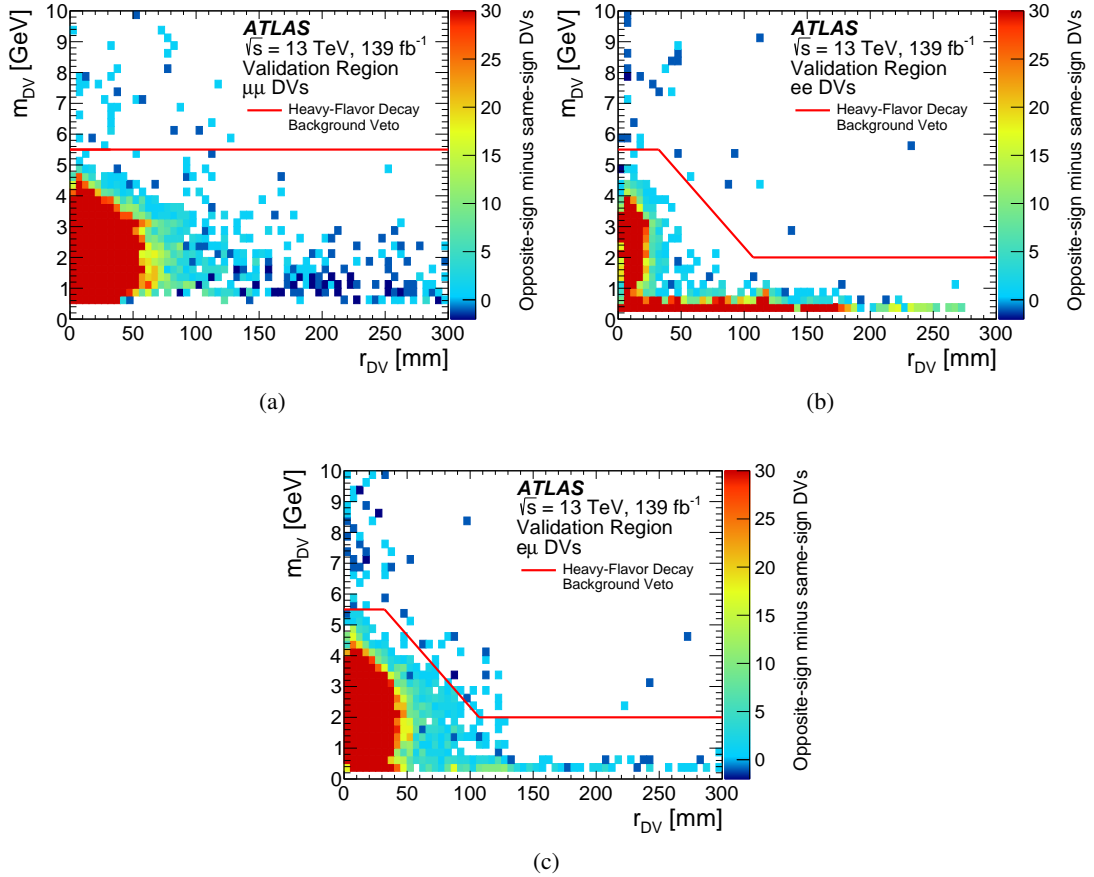
11

Figure 5: The two-dimensional distribution of m_{DV} and r_{DV}. Shown is the difference between the OS- and SS-vertex distributions. The vertices used in the selection are from the validation region, in which events containing prompt leptons are vetoed. The z-axis maximum is set to 30 to provide a scale that distinguishes between small positive (more OS- than SS-DVs) and small negative (more SS- than OS-DVs) entries. The solid red line represents the DV selection that is applied in each channel to remove background from heavy-flavor decays. The larger reconstruction efficiency for $\mu\mu$ DVs results in a number of displaced $J/\psi \rightarrow \mu\mu$ decays. For this reason, the r_{DV}–m_{DV} correlation selection, which is applied in the ee and $e\mu$ channels, is not sufficient to remove heavy-flavor $\mu\mu$ decays. Instead, an $m_{DV} > 5.5$ GeV selection is applied in channels with $\mu\mu$ DVs.

A HNL mass

The HNL mass (m_{HNL}) can be obtained using energy–momentum conservation in the HNL production ($W \to \mathcal{N}\ell_1$) and decay ($\mathcal{N} \to \ell_2\ell_3\nu$), where ℓ_1 is the prompt lepton and ℓ_2 and ℓ_3 are the charged leptons in the DV. The problem can be summarized with the following equations. Four-momentum conservation in the $\mathcal{N}$ decay gives

$$p_{\mathcal{N}}^{\mu} = p_2^{\mu} + p_3^{\mu} + p_{\nu}^{\mu} \equiv p_{23}^{\mu} + p_{\nu}^{\mu}. \tag{1}$$

Four-momentum conservation in the W decay gives

$$p_W^{\mu} = p_1^{\mu} + p_{\mathcal{N}}^{\mu} = p_1^{\mu} + p_{23}^{\mu} + p_{\nu}^{\mu}. \tag{2}$$

The following are defined

$$
\begin{aligned}
p_{23}^2 &= E_{23}^2 - |\vec{p}_{23}|^2 \equiv m_{23}^2 \\
p_{23}^{\parallel} &\equiv \vec{p}_{23} \cdot \hat{v} \\
p_{23}^{\perp} &\equiv |\vec{p}_{23} - p_{23}^{\parallel}\hat{v}|
\end{aligned}
$$

where m, E, and $|\vec{p}|$ are the mass, energy, and momentum-vector magnitude of the particles indicated by their subscript and $\hat{v}$ is the flight direction of the HNL given by the vector connecting the PV and DV.

The solution to the HNL mass is presented in the coordinate system $k = (\hat{x}', \hat{y}', \hat{z}')$, which is rotated relative to the ATLAS coordinate system, such that the origin of the k-frame is at the PV and the z'-axis points along the flight direction of the HNL. The definition of this coordinate system is

$$\hat{z}' = \hat{v}, \quad \hat{x}' = \frac{\vec{p}_{23} \times \hat{z}'}{|\vec{p}_{23} \times \hat{z}'|}, \quad \hat{y}' = \hat{z}' \times \hat{x}'.$$

The momenta of ℓ_2 and ℓ_3 constrain the components of the neutrino momentum orthogonal to $\vec{p}_{\mathcal{N}}$. This means that energy–momentum conservation in the W and $\mathcal{N}$ decays can be expressed in terms of one unknown variable α, which is the component of neutrino momentum in the $\hat{z}'$ direction. To express Eqs. (1) and (2) in terms of α, the following quantities are defined

$$\vec{p}'_{23} \equiv \vec{q} \tag{3}$$
$$\vec{q} = (0, |\vec{p}_{23} \times \hat{z}'| \equiv q_{\perp}, \vec{p}_{23} \cdot \hat{z}' \equiv q_z) \tag{4}$$
$$\vec{p}'_{\nu} = (0, -q_{\perp}, \alpha) \tag{5}$$
$$E'_{\nu} = \sqrt{q_{\perp}^2 + \alpha^2}. \tag{6}$$

Squaring Eq. (2) gives

$$p_W'^2 = m_W^2 = m_1^2 + m_{\nu}^2 + m_{23}^2 + 2p_1' \cdot (p_{23}' + p_{\nu}') + 2p_{23}' \cdot p_{\nu}' \tag{7}$$

where

$$p'_1 \cdot (p'_{23} + p'_\nu) = E'_1(E'_{23} + E'_\nu) - p'_{1,z}(q_z + \alpha)$$
$$p'_{23} \cdot p'_\nu = E'_{23}E'_\nu + q_\perp^2 - q_z\alpha.$$

In the energy regime of interest, the charged leptons and neutrino can be treated as massless particles, such that $m_1 = m_\nu = 0$. Rearranging Eq. (7) to solve for E_ν gives

$$E'_\nu = A + B\alpha \tag{8}$$

where

$$A = \frac{(m_W^2 - m_{23}^2)/2 - E'_1 E'_{23} + p'_{1,z} q_z - q_\perp^2}{E'_1 + E'_{23}}, \quad B = \frac{p'_{1,z} + q_z}{E'_1 + E'_{23}}$$

Subtracting Eq. (8) from Eq. (6) gives the following quadratic expression in α

$$(B^2 - 1)\alpha^2 + 2AB\alpha + A^2 - q_\perp^2 = 0.$$

The solution for α is therefore

$$\alpha = \frac{-AB \pm \sqrt{(B^2 - 1)q_\perp^2 + A^2}}{(B^2 - 1)}. \tag{9}$$

Both solutions for α were studied using simulated HNL events and it was noted that the solution that led to a smaller $|\vec{p}_N|$ typically led to a value for m_{HNL} that was closer to the simulated m_N. This solution often corresponded to forward emission of the neutrino with respect to the HNL decay. Therefore, the definition of m_{HNL} in the analysis uses the solution with the positive radical.

The expression for α in Eq. (9) depends on m_W. ATLAS has measured the W-boson pole mass to be $M_W = 80.370 \pm 0.019$ GeV [75]. This measurement is combined in Ref. [2] with results from other collider experiments to provide a measurement of the W-boson width, $\Gamma_W = 2.195 \pm 0.083$ GeV. Since the W mass has a width, then if $m_W = M_W$ in Eq. (9) it is possible that there is no real solution for α. Instead of rejecting these events, m_W is set equal to the median W mass in the kinematically allowed region ($m_{W,\mathrm{med}}$). This ensures that α (and correspondingly m_{HNL}) always has a real solution.

To define the kinematically allowed region, the minimum W mass that is consistent with the charged-lepton decay products ($m_{W,\mathrm{min}}$) is computed. From Eq. (7), the mass of the W boson is given by

$$m_W^2 = m_{23}^2 + 2\left(E'_1 E'_{23} + E'_\nu(E'_1 + E'_{23}) - p'_{1,z} q_z + q_\perp^2 - \alpha(p'_{1,z} + q_z)\right) \tag{10}$$

and $m_{W,\mathrm{min}}$ occurs where

$$\frac{d(m_W^2/2)}{d\alpha} = (E'_1 + E'_{23})\frac{dE'_\nu}{d\alpha} - (p'_{1,z} + q_z) = 0. \tag{11}$$

Using

$$\frac{dE'_\nu}{d\alpha} = \frac{d\sqrt{q_\perp^2 + \alpha^2}}{d\alpha} = \frac{\alpha}{E'_\nu}$$

in Eq. (11), the chosen value of α that gives the minimum m_W is

$$\alpha = \frac{q_\perp B}{\sqrt{1 - B^2}}. \tag{12}$$

Substituting Eq. (12) into Eq. (10), the minimum W boson mass is

$$m_{W,\text{min}}^2 = m_{23}^2 + 2\left(E'_1 E'_{23} + (E'_1 + E'_{23})\sqrt{q_\perp^2 + \frac{q_\perp^2 B^2}{1 - B^2}} - p'_{1,z} q_z + q_\perp^2 - (p'_{1,z} + q_z)\frac{q_\perp B}{\sqrt{1 - B^2}} \right).$$

The cumulative probability for the W boson to have a mass greater than $m_{W,\text{min}}$ is used to find the median of the remaining distribution. The probability density function (f) for m_W^2 satisfies

$$f(m_W^2) \propto \frac{1}{(m_W^2 - M_W^2)^2 + M_W^2 \Gamma_W^2}.$$

Therefore, the cumulative distribution function (F) is

$$F(m_W^2) = \frac{1}{\pi} \arctan\left(\frac{m_W^2 - M_W^2}{M_W \Gamma_W} \right) + \frac{1}{2}. \tag{13}$$

The midpoint of the allowed kinematic region has a value of

$$F_{\text{med}} = \frac{1 + F(m_{W,\text{min}}^2)}{2}$$

Rearranging Eq. (13) for m_W^2 gives

$$m_W^2 = M_W^2 + \Gamma_W M_W \tan\left(\pi \left[F - \frac{1}{2} \right] \right). \tag{14}$$

Substituting $F = F_{\text{med}}$ in Eq. (14) gives an expression for the median W mass in the kinematically allowed region

$$m_{W,\text{med}}^2 = M_W^2 + \Gamma_W M_W \tan\left(\pi \left[\frac{1 + F(m_{W,\text{min}}^2)}{2} - \frac{1}{2} \right] \right).$$

This value of $m_{W,\text{med}}$ is used in Eq. (9) to solve for α.

From Eq. (1) and the definitions in Eqs. (3) to (6), the expression for the HNL mass in terms of α is

$$
\begin{aligned}
m_{\text{HNL}}^2 &= m_{23}^2 + 2p'_\nu \cdot p'_{23} \\
&= m_{23}^2 + 2E'_{23}\sqrt{q_\perp^2 + \alpha^2} + 2q_\perp^2 - 2q_z\alpha.
\end{aligned}
\tag{15}
$$

Substituting the expression for α in Eq. (9) into Eq. (15) gives the solution for the HNL mass.

References

[1] P. F. de Salas, D. V. Forero, C. A. Ternes, M. Tortola, and J. W. F. Valle,
Status of neutrino oscillations 2018: 3σ hint for normal mass ordering and improved CP sensitivity,
Phys. Lett. B **782** (2018) 633, arXiv: 1708.01186 [hep-ph].

[2] Particle Data Group Collaboration, *Review of Particle Physics*, PTEP **2020** (2020) 083C01.

[3] P. Minkowski, $\mu \to e\gamma$ *at a rate of one out of* 10^9 *muon decays*, Phys. Lett. B **67** (1977) 421.

[4] T. Yanagida, *Horizontal gauge symmetry and masses of neutrinos*,
Conf. Proc. C **7902131** (1979) 95, ed. by O. Sawada and A. Sugamoto.

[5] S. L. Glashow, *The Future of Elementary Particle Physics*, NATO Sci. Ser. B **61** (1980) 687.

[6] M. Gell-Mann, P. Ramond, and R. Slansky, *Complex Spinors and Unified Theories*,
Conf. Proc. C **790927** (1979) 315, arXiv: 1306.4669 [hep-th].

[7] R. N. Mohapatra and G. Senjanovic, *Neutrino Mass and Spontaneous Parity Nonconservation*,
Phys. Rev. Lett. **44** (1980) 912.

[8] J. Schechter and J. W. F. Valle, *Neutrino Masses in SU(2) x U(1) Theories*,
Phys. Rev. D **22** (1980) 2227.

[9] J. Schechter and J. W. F. Valle, *Neutrino Decay and Spontaneous Violation of Lepton Number*,
Phys. Rev. D **25** (1982) 774.

[10] S. Davidson, E. Nardi, and Y. Nir, *Leptogenesis*, Phys. Rept. **466** (2008) 105,
arXiv: 0802.2962 [hep-ph].

[11] A. Pilaftsis, *The little review on leptogenesis*, J. Phys. Conf. Ser. **171** (2009) 012017,
arXiv: 0904.1182 [hep-ph].

[12] M. Shaposhnikov, *Baryogenesis*, J. Phys. Conf. Ser. **171** (2009) 012005.

[13] E. K. Akhmedov, V. A. Rubakov, and A. Y. Smirnov, *Baryogenesis via neutrino oscillations*,
Phys. Rev. Lett. **81** (1998) 1359, arXiv: hep-ph/9803255.

[14] T. Asaka, S. Blanchet, and M. Shaposhnikov, *The νMSM, dark matter and neutrino masses*,
Phys. Lett. B **631** (2005) 151, arXiv: hep-ph/0503065 [hep-ph].

[15] M. Drewes et al., *ARS Leptogenesis*, Int. J. Mod. Phys. A **33** (2018) 1842002,
arXiv: 1711.02862 [hep-ph].

[16] J. Klarić, M. Shaposhnikov, and I. Timiryasov, *Uniting Low-Scale Leptogenesis Mechanisms*,
Phys. Rev. Lett. **127** (2021) 111802, arXiv: 2008.13771 [hep-ph].

[17] J. Klarić, M. Shaposhnikov, and I. Timiryasov,
Reconciling resonant leptogenesis and baryogenesis via neutrino oscillations,
Phys. Rev. D **104** (2021) 055010, arXiv: 2103.16545 [hep-ph].

[18] T. Asaka and M. Shaposhnikov, *The νMSM, dark matter and baryon asymmetry of the universe*,
Phys. Lett. B **620** (2005) 17, arXiv: hep-ph/0505013 [hep-ph].

[19] A. Boyarsky, O. Ruchayskiy, and M. Shaposhnikov,
The Role of sterile neutrinos in cosmology and astrophysics,
Ann. Rev. Nucl. Part. Sci. **59** (2009) 191, arXiv: 0901.0011 [hep-ph].

[20] A. Boyarsky, M. Drewes, T. Lasserre, S. Mertens, and O. Ruchayskiy, *Sterile neutrino Dark Matter*,
Prog. Part. Nucl. Phys. **104** (2019) 1, arXiv: 1807.07938 [hep-ph].

[21] J. Ghiglieri and M. Laine, *Sterile neutrino dark matter via coinciding resonances*, JCAP **07** (2020) 012, arXiv: `2004.10766 [hep-ph]`.

[22] ATLAS Collaboration, *Search for heavy neutral leptons in decays of W bosons produced in* 13 *TeV pp collisions using prompt and displaced signatures with the ATLAS detector*, JHEP **10** (2019) 265, arXiv: `1905.09787 [hep-ex]`.

[23] Belle Collaboration, *Search for heavy neutrinos at Belle*, Phys. Rev. D **87** (2013) 071102, [Erratum: Phys. Rev. D **95**, 099903 (2017)], arXiv: `1301.1105 [hep-ex]`.

[24] NuTeV Collaboration, *Search for neutral heavy leptons in a high-energy neutrino beam*, Phys. Rev. Lett. **83** (1999) 4943, arXiv: `hep-ex/9908011`.

[25] DELPHI Collaboration, *Search for neutral heavy leptons produced in Z decays*, Z. Phys. C **74** (1997) 57, [Erratum: Z. Phys. C **75**, 580 (1997)].

[26] CHARM II Collaboration, *Search for heavy isosinglet neutrinos*, Phys. Lett. B **343** (1995) 453.

[27] NA3 Collaboration, *Mass and lifetime limits on new long-lived particles in 300 GeV/c π^- interactions*, Z. Phys. C **31** (1986) 21.

[28] CHARM Collaboration, *A search for decays of heavy neutrinos in the mass range 0.5-2.8 GeV*, Phys. Lett. B **166** (1986) 473.

[29] WA66 Collaboration, *Search for heavy neutrino decays in the BEBC beam dump experiment*, Phys. Lett. B **160** (1985) 207.

[30] CMS Collaboration, *Search for long-lived heavy neutral leptons with displaced vertices in proton-proton collisions at $\sqrt{s}$ =13 TeV*, (2022), arXiv: `2201.05578 [hep-ex]`.

[31] M. Shaposhnikov, *A possible symmetry of the νMSM*, Nucl. Phys. B **763** (2007) 49, arXiv: `hep-ph/0605047`.

[32] J. Kersten and A. Y. Smirnov, *Right-Handed Neutrinos at CERN LHC and the Mechanism of Neutrino Mass Generation*, Phys. Rev. D **76** (2007) 073005, arXiv: `0705.3221 [hep-ph]`.

[33] J.-L. Tastet, O. Ruchayskiy, and I. Timiryasov, *Reinterpreting the ATLAS bounds on heavy neutral leptons in a realistic neutrino oscillation model*, JHEP **12** (2021) 182, arXiv: `2107.12980 [hep-ph]`.

[34] M. Gronau, C. N. Leung, and J. L. Rosner, *Extending Limits on Neutral Heavy Leptons*, Phys. Rev. D **29** (1984) 2539.

[35] K. Bondarenko, A. Boyarsky, D. Gorbunov, and O. Ruchayskiy, *Phenomenology of GeV-scale Heavy Neutral Leptons*, JHEP **11** (2018) 032, arXiv: `1805.08567 [hep-ph]`.

[36] *See Supplemental Material at [URL will be inserted by publisher]*, ().

[37] T. Sjöstrand et al., *An introduction to PYTHIA 8.2*, Comput. Phys. Commun. **191** (2015) 159, arXiv: `1410.3012 [hep-ph]`.

[38] ATLAS Collaboration, *ATLAS Pythia 8 tunes to* 7 *TeV data*, ATL-PHYS-PUB-2014-021, 2014, URL: `https://cds.cern.ch/record/1966419`.

[39] R. D. Ball et al., *Parton distributions with LHC data*, Nucl. Phys. B **867** (2013) 244, arXiv: 1207.1303 [hep-ph].

[40] ATLAS Collaboration, *The Pythia 8 A3 tune description of ATLAS minimum bias and inelastic measurements incorporating the Donnachie–Landshoff diffractive model*, ATL-PHYS-PUB-2016-017, 2016, URL: https://cds.cern.ch/record/2206965.

[41] ATLAS Collaboration, *The ATLAS Simulation Infrastructure*, Eur. Phys. J. C **70** (2010) 823, arXiv: 1005.4568 [physics.ins-det].

[42] GEANT4 Collaboration, S. Agostinelli, et al., *GEANT4 – a simulation toolkit*, Nucl. Instrum. Meth. A **506** (2003) 250.

[43] J.-L. Tastet and I. Timiryasov, *Dirac vs. Majorana HNLs (and their oscillations) at SHiP*, JHEP **04** (2020) 005, arXiv: 1912.05520 [hep-ph].

[44] R. Ruiz, *Quantitative study on helicity inversion in Majorana neutrino decays at the LHC*, Phys. Rev. D **103** (2021) 015022, arXiv: 2008.01092 [hep-ph].

[45] J. Alwall et al., *The automated computation of tree-level and next-to-leading order differential cross sections, and their matching to parton shower simulations*, JHEP **07** (2014) 079, arXiv: 1405.0301 [hep-ph].

[46] C. Degrande, O. Mattelaer, R. Ruiz, and J. Turner, *Fully automated precision predictions for heavy neutrino production mechanisms at hadron colliders*, Phys. Rev. D **94** (2016) 053002, arXiv: 1602.06957 [hep-ph].

[47] S. Pascoli, R. Ruiz, and C. Weiland, *Heavy neutrinos with dynamic jet vetoes: multilepton searches at $\sqrt{s} = 14$, 27, and 100 TeV*, JHEP **06** (2019) 049, arXiv: 1812.08750 [hep-ph].

[48] ATLAS Collaboration, *The ATLAS Experiment at the CERN Large Hadron Collider*, JINST **3** (2008) S08003.

[49] ATLAS Collaboration, *ATLAS Insertable B-Layer: Technical Design Report*, ATLAS-TDR-19; CERN-LHCC-2010-013, 2010, URL: https://cds.cern.ch/record/1291633, Addendum: ATLAS-TDR-19-ADD-1; CERN-LHCC-2012-009, 2012, URL: https://cds.cern.ch/record/1451888.

[50] B. Abbott et al., *Production and integration of the ATLAS Insertable B-Layer*, JINST **13** (2018) T05008, arXiv: 1803.00844 [physics.ins-det].

[51] ATLAS Collaboration, *The ATLAS Collaboration Software and Firmware*, ATL-SOFT-PUB-2021-001, 2021, URL: https://cds.cern.ch/record/2767187.

[52] ATLAS Collaboration, *Performance of the ATLAS trigger system in 2015*, Eur. Phys. J. C **77** (2017) 317, arXiv: 1611.09661 [hep-ex].

[53] ATLAS Collaboration, *Performance of electron and photon triggers in ATLAS during LHC Run 2*, Eur. Phys. J. C **80** (2020) 47, arXiv: 1909.00761 [hep-ex].

[54] ATLAS Collaboration, *Performance of the ATLAS muon triggers in Run 2*, JINST **15** (2020) P09015, arXiv: 2004.13447 [hep-ex].

[55] ATLAS Collaboration, *Muon reconstruction and identification efficiency in ATLAS using the full Run 2 pp collision data set at $\sqrt{s} = 13$ TeV*, Eur. Phys. J. C **81** (2021) 578, arXiv: 2012.00578 [hep-ex].

[56] ATLAS Collaboration, *Electron and photon performance measurements with the ATLAS detector using the 2015–2017 LHC proton–proton collision data*, JINST **14** (2019) P12006, arXiv: 1908.00005 [hep-ex].

[57] ATLAS Collaboration,
Performance of the reconstruction of large impact parameter tracks in the inner detector of ATLAS,
ATL-PHYS-PUB-2017-014, 2017, URL: https://cds.cern.ch/record/2275635.

[58] ATLAS Collaboration, *Performance of the ATLAS track reconstruction algorithms in dense environments in LHC Run 2*,
Eur. Phys. J. C **77** (2017) 673, arXiv: 1704.07983 [hep-ex].

[59] ATLAS Collaboration,
Performance of vertex reconstruction algorithms for detection of new long-lived particle decays within the ATLAS inner detector, ATL-PHYS-PUB-2019-013, 2019,
URL: https://cds.cern.ch/record/2669425.

[60] ATLAS Collaboration,
Search for displaced leptons in $\sqrt{s} = 13$ TeV pp collisions with the ATLAS detector,
Phys. Rev. Lett. **127** (2020) 051802, arXiv: 2011.07812 [hep-ex].

[61] ATLAS Collaboration, *Search for displaced vertices of oppositely charged leptons from decays of long-lived particles in pp collisions at $\sqrt{s} = 13$ TeV with the ATLAS detector*,
Phys. Lett. B **801** (2020) 135114, arXiv: 1907.10037 [hep-ex].

[62] ATLAS Collaboration, *Search for long-lived, massive particles in events with displaced vertices and missing transverse momentum in $\sqrt{s} = 13$ TeV pp collisions with the ATLAS detector*,
Phys. Rev. D **97** (2018) 052012, arXiv: 1710.04901 [hep-ex].

[63] ATLAS Collaboration, *Search for exotic decays of the Higgs boson into long-lived particles in pp collisions at $\sqrt{s} = 13$ TeV using displaced vertices in the ATLAS inner detector*,
JHEP **11** (2021) 229, arXiv: 2107.06092 [hep-ex].

[64] ATLAS Collaboration,
Early Inner Detector Tracking Performance in the 2015 Data at $\sqrt{s} = 13$ TeV,
ATL-PHYS-PUB-2015-051, 2015, URL: https://cds.cern.ch/record/2110140.

[65] ATLAS Collaboration, *Muon reconstruction performance of the ATLAS detector in proton–proton collision data at $\sqrt{s} = 13$ TeV*, Eur. Phys. J. C **76** (2016) 292, arXiv: 1603.05598 [hep-ex].

[66] ATLAS Collaboration, *Measurement of $W^\pm$ and Z-boson production cross sections in pp collisions at $\sqrt{s} = 13$ TeV with the ATLAS detector*, Phys. Lett. B **759** (2016) 601,
arXiv: 1603.09222 [hep-ex].

[67] M. Davier, A. Hocker, and Z. Zhang, *The Physics of Hadronic Tau Decays*,
Rev. Mod. Phys. **78** (2006) 1043, arXiv: hep-ph/0507078.

[68] ATLAS Collaboration,
Luminosity determination in pp collisions at $\sqrt{s} = 13$ TeV using the ATLAS detector at the LHC,
ATLAS-CONF-2019-021, 2019, URL: https://cds.cern.ch/record/2677054.

[69] G. Avoni et al., *The new LUCID-2 detector for luminosity measurement and monitoring in ATLAS*,
JINST **13** (2018) P07017.

[70] A. L. Read, *Presentation of search results: the CL_S technique*, J. Phys. G **28** (2002) 2693.

[71] L. Moneta et al., *The RooStats Project*, PoS **ACAT2010** (2010) 057,
arXiv: 1009.1003 [physics.data-an].

[72] W. Verkerke and D. P. Kirkby, *The RooFit toolkit for data modeling*,
eConf **C0303241** (2003) MOLT007, arXiv: `physics/0306116`.

[73] K. Cranmer, G. Lewis, L. Moneta, A. Shibata, and W. Verkerke,
HistFactory: A tool for creating statistical models for use with RooFit and RooStats, tech. rep.,
New York U., 2012, URL: `https://cds.cern.ch/record/1456844`.

[74] P. Agrawal et al., *Feebly-interacting particles: FIPs 2020 workshop report*,
Eur. Phys. J. C **81** (2021) 1015, arXiv: `2102.12143 [hep-ph]`.

[75] ATLAS Collaboration,
Measurement of the W-boson mass in pp collisions at $\sqrt{s} = 7$ TeV with the ATLAS detector,
Eur. Phys. J. C **78** (2018) 110, arXiv: `1701.07240 [hep-ex]`,
Erratum: Eur. Phys. J. C **78** (2018) 898.